

# Non-Markovian behaviour and the dual role of astrocytes in Alzheimer’s disease development and propagation

Swadesh Pal<sup>a,\*</sup>, Roderick Melnik<sup>a,b</sup>

<sup>a</sup>MS2 Discovery Interdisciplinary Research Institute, Wilfrid Laurier University, Waterloo, Canada

<sup>b</sup>BCAM - Basque Center for Applied Mathematics, E-48009, Bilbao, Spain

---

## Abstract

Alzheimer’s disease (AD) is a common neurodegenerative disorder nowadays. Amyloid-beta ( $A\beta$ ) and tau proteins are among the main contributors to the development or propagation of AD. In AD,  $A\beta$  proteins clump together to form plaques and disrupt cell functions. On the other hand, the abnormal chemical change in the brain helps to build sticky tau tangles that block the neuron’s transport system. Astrocytes generally maintain a healthy balance in the brain by clearing the  $A\beta$  plaques (toxic  $A\beta$ ). However, over-activated astrocytes release chemokines and cytokines in the presence of  $A\beta$  and react to pro-inflammatory cytokines, further increasing the production of  $A\beta$ . In this paper, we construct a mathematical model that can capture astrocytes’ dual behaviour. Furthermore, we reveal that the disease propagation depends on the current time instance and the disease’s earlier status, called the “memory effect”. We consider a fractional order network mathematical model to capture the influence of such memory effect on AD propagation. We have integrated brain connectome data into the model and studied the memory effect, the dual role of astrocytes, and the brain’s neuronal damage. Based on the pathology, primary, secondary, and mixed tauopathies parameters are considered in the model. Due to the mixed tauopathy, different brain nodes or regions in the brain connectome accumulate different toxic concentrations of  $A\beta$  and tau proteins. Finally, we explain how the memory effect can slow down the propagation of such toxic proteins in the brain, decreasing the rate of neuronal damage.

*Keywords:* Alzheimer’s disease, Astrocytes, Non-Markovian process, Caputo fractional derivatives, Network model, Brain connectome

---

## 1. Introduction

Alzheimer’s disease (AD) is a progressive and irreversible neurodegenerative disorder that affects memory, thinking, and behaviours. These cognitive declines may be so severe that they interfere with daily tasks. Dr. Alois Alzheimer first observed this disease in 1906 and described it as “a peculiar disease” [1]. He examined a woman’s brain who had died of an unusual mental illness, including memory loss and language problems. He found many abnormal clumps (amyloid-beta plaques) and fibre bundle tangles (tau tangles), which are now considered as one of the main contributors to AD development [1, 2, 3]. Researchers believe they block communication between nerve cells, disrupt many processes, and cause memory loss, difficulty in speaking and other cognitive declines.

---

\*Swadesh Pal

Email addresses: spal@wlu.ca (Swadesh Pal), rmelnik@wlu.ca (Roderick Melnik)

AD is not a normal part of ageing, but the risk factor of getting the disease increases with age [4, 5]. Most AD-affected people are 65 years of age or over, but it is possible to have the disease before age 65, referred to as early-onset Alzheimer's [6]. At the early stage of the disease, the AD-affected people's memory loss is mild, but over age, they gradually lose their ability to carry on a conversation or recognition. Depending on different factors, AD-affected people can live 20 years after diagnosis, but on average, they live 8 to 10 years [7, 8]. To date, AD has no cure except for a few medications, such as aducanumab, that can help to reduce cognitive decline at the early stage of the disease [9, 10, 11]. Many researchers have been working worldwide to understand the disease in a better way and prevent it from spreading.

Accumulation of amyloid-beta ( $A\beta$ ) in the extracellular space is often considered to be one of the main initiators of the early onset of AD [12, 13, 14, 15, 16]. This accumulation may happen due to its overproduction or the lower clearance rate [17].  $A\beta$  comprises 39-43 amino acids with different biophysical states, and soluble  $A\beta_{40}$  and insoluble  $A\beta_{42}$  are the two major isoforms that have been observed in the brain. In a healthy brain, more than 90% concentration of  $A\beta$  is observed in the form of  $A\beta_{40}$  while less than 5% is found in the form of  $A\beta_{42}$  [18, 19, 20]. However, an AD-affected brain cannot maintain this type of healthy balance and a higher concentration of  $A\beta_{42}$  peptide causes the forming of plaques and disrupts normal cell function. Another important key factor of AD is the tau protein ( $\tau$ P) [21, 22]. The normal  $\tau$ P forms a microtubule, and they help in transporting nutrients and other substances from one part of a nerve cell to another [23]. Due to abnormal chemical changes in the brain, the tau protein detaches from microtubules and sticks to other  $\tau$ P [24, 25]. This causes the tau protein to form neurofibrillary tangles (misfolded and abnormally shaped) inside neurons and block the neuron's transport system.

Researchers have been focused on identifying the concentrations of  $A\beta$  and  $\tau$ P at the early onset of AD. To date, the accumulation of these proteins is not yet fully measurable with blood tests and can not be visualized on CT or MRI scans. The FDA-approved amyloid PET scan tracer can identify the presence of AD but cannot measure the disease progression fully, so this has been used only for clinical trials [26, 27, 28]. On the other hand, F-18 flortaucipir is the first FDA-approved tau PET scan tracer, and it helps in the stage of AD neurodegeneration [29, 30]. Along with these two proteins, many other factors influence AD development and progression. Substantial efforts have been made to identify the disease state concerning such different factors.

Astrocytes are the largest and most numerous types of glial cells in the central nervous system (CNS), as they serve as an immunodefense to the CNS. They regulate blood flow, transfer mitochondria to neurons, and help in neuronal metabolism [31, 32, 33, 34]. Generally, activated astrocytes clear debris from the brain and protect neurons from disease [35, 36, 37, 38]. But, in the AD-affected brain, they lose the ability to maintain a healthy balance and support AD propagation [39]. In the early stages of AD, a sufficient amount of toxic amyloid-beta mainly disrupts this healthy balance. In this case, astrocytes can not control the ionic balance in the brain, in particular, intracellular  $Ca^{2+}$  concentrations. As a result, NADPH oxidase (NOX) is stimulated, and neuronal death happens through oxidative stress [40, 41]. Many other negative effects occur due to the over-activation of astrocytes, such as apolipoprotein E (ApoE) and the excess production of glutamate. For example, one of the neurotoxic isoforms ApoE4 of ApoE supports toxic  $A\beta$  deposition in the initial stage of AD development [6, 42].

One of the main aspects of our current work is to analyze astrocytes' dual role before and after AD. We constructed a mathematical model incorporating the role of astrocytes in AD along with the  $A\beta$  and  $\tau$ P interactions. Each of these proteins ( $A\beta$  and  $\tau$ P) follows a modified heterodimer model for protein-protein interactions in the reaction kinetics with a coupling parameter between them [43]. We modify the exponential growth by logistic growth in the growth term for both the healthy proteins' equation [44, 45]. We consider a logistic growth in the astrocytes equation and assume that they clear toxic amyloid beta

[46, 47]. Furthermore, these toxic proteins damage the neurons in the brain connectome. The amount of neuronal damage is studied here by the coupling of toxic  $A\beta$  and  $\tau P$ , which also gives the disease status in the brain [43].

Researchers have been considering different modelling approaches so that an expert can extract more and more information from available data. One such approach is fractional calculus; it captures memory effects, fractality, multiscale nature and better data fitting. Due to its global correlation, it can reflect the historical process of the systematic function. Regarding the data fitting, it has been observed that the fractional model has one more degree of freedom than the integer-order model [48]. Given that a reaction-diffusion process can depend not only on the previous time instance's concentrations but also on all the earlier stages of the concentrations with some weights [49, 50, 51, 52, 53, 54], this idea is further developed in this paper. A time-fractional reaction-diffusion equation, collectively called the "memory effect", is used to analyze such processes in the AD context. Studying this type of memory effect in Alzheimer's disease is very important as the disease spread rate or recovery rate for different individuals is different, e.g., the recovery rate for an individual who has been suffering the disease for twenty years is not the same for another individual who is having the disease for ten years. The Caputo derivative is one of the most appropriate fractional operators used in such modelling, which has many other real-world applications [52, 55, 56]. In this work, we first construct a time-fractional partial differential equation (PDE) model to describe the AD progression. Then, we derive the network model corresponding to the PDE model so that we can integrate the brain connectivity data and analyze the damage dynamics concerning the memory effect. Different tauopathies have been studied for the network model to incorporate different scenarios depending on the toxic  $A\beta$  and toxic  $\tau P$ . Furthermore, we have compared the disease propagation in the presence and absence of memories on nodes and in brain connectome regions.

The rest of this paper is organized as follows. In Sect. 2, we formulate the temporal models for AD progression for both cases: absence and presence of memories. The equilibrium points and their stabilities for the temporal model are discussed in Sect. 3. In Sect. 4, we extend the temporal model in a subset of Euclidean space and then into the network to integrate brain connectome data. Exhaustive numerical simulation results are presented in Sect. 5 to analyze the dual role of astrocytes and the memory effect in AD progression. Finally, the conclusions and future directions are presented in Sect. 6.

## 2. Model Formulation

Astrocytes are the glial cells present in the central nervous system, and they have been very closely associated with the development of Alzheimer's disease (AD) in the brain [57]. To capture the dual role of astrocytes in healthy and AD-affected brains, we introduce an equation corresponding to astrocytes and modify the temporal model defined in [43, 45] as

$$\frac{du}{dt} = u(a_0 - a_1u) - a_2u\tilde{u}, \quad (1a)$$

$$\frac{d\tilde{u}}{dt} = -\tilde{a}_1\tilde{u} + a_2u\tilde{u} - \mu\tilde{u}(w - \tilde{u}), \quad (1b)$$

$$\frac{dv}{dt} = v(b_0 - b_1v) - b_2v\tilde{v} - b_3\tilde{u}v\tilde{v}, \quad (1c)$$

$$\frac{d\tilde{v}}{dt} = -\tilde{b}_1\tilde{v} + b_2v\tilde{v} + b_3\tilde{u}v\tilde{v}, \quad (1d)$$

$$\frac{dw}{dt} = w(c_0 - w/c_1), \quad (1e)$$

where  $u$  and  $\tilde{u}$  are the healthy and toxic densities of the protein  $A\beta$  and  $v$  and  $\tilde{v}$  are the healthy and toxic densities for  $\tau P$ . The parameters  $a_0$  and  $b_0$  are the mean production rates of healthy proteins,  $a_1$ ,  $b_1$ ,  $\tilde{a}_1$  and  $\tilde{b}_1$  are the mean clearance rates of healthy and toxic proteins, and  $a_2$  and  $b_2$  represent the mean conversion rates of healthy proteins to toxic proteins. Here, the parameter  $b_3$  represents the coupling between the two proteins  $A\beta$  and  $\tau P$ . The variable  $w$  represents the concentration of astrocytes with  $c_0$  as the production rate and the term  $c_0 c_1$  as the saturation point. The parameter  $\mu$  is responsible for the dual role of astrocytes. If  $w > \tilde{u}$ , then astrocytes clear the concentrations of the toxic amyloid-beta; otherwise, it helps to increase the toxic concentrations.

For any time  $t > 0$ , the concentration of the substances depends on the reaction terms on the right-hand side of the equation (1). Practically, it means that an individual who has had dementia for twenty years has the same chance of clearing Alzheimer's as someone who had dementia less than ten years ago. It is an assumption based on the Markovian process, which is not generally valid. Non-Markovian processes have been playing an increasingly important role in studying living systems [58, 59], and neuroscience research is no exception where such processes have to be incorporated in state-of-the-art models of neurodegenerative diseases. Clearly, the concentrations of the substances we discussed above not only depend on the time instance  $t$ ; rather, they depend on some weighted average concentrations of pastime interval, say  $[t_p, t]$  for  $t_p < t$ . This is usually termed collectively as the memory effect [50, 51, 52, 54, 56]. The distribution of the weights is proportional to some power of the length of the time interval, i.e.,  $(t - t_p)$ , following the power law correlation function [49, 52]. Without the loss of generality, we can choose  $t_p = 0$ . Now, incorporating these into the mathematical model, we obtain the fractional order differential equations as

$$D_t^\alpha u = u(a_0 - a_1 u) - a_2 u \tilde{u}, \quad (2a)$$

$$D_t^\alpha \tilde{u} = -\tilde{a}_1 \tilde{u} + a_2 u \tilde{u} - \mu \tilde{u}(w - \tilde{u}), \quad (2b)$$

$$D_t^\alpha v = v(b_0 - b_1 v) - b_2 v \tilde{v} - b_3 \tilde{u} v \tilde{v}, \quad (2c)$$

$$D_t^\alpha \tilde{v} = -\tilde{b}_1 \tilde{v} + b_2 v \tilde{v} + b_3 \tilde{u} v \tilde{v}, \quad (2d)$$

$$D_t^\alpha w = w(c_0 - w/c_1), \quad (2e)$$

where  $D_t^\alpha z(t)$  stands for the Caputo fractional derivative that is defined by

$$D_t^\alpha z(t) = \frac{1}{\Gamma(1 - \alpha)} \int_0^t \frac{z'(s)}{(t - s)^\alpha} ds, \quad 0 < \alpha < 1,$$

and  $z'$  denotes the first-order derivative of  $z$ . Here in the modified fractional differential model (2), the influence of memory decreases when  $\alpha \rightarrow 1$ , and the system tends toward a memoryless system [52, 60]. In addition, the accumulations of toxic amyloid-beta and tau proteins cause neuronal damage. We consider the memory effect in such neuronal damage equation by modelling it by the following equation:

$$D_t^\alpha q = (k_1 \tilde{u} + k_2 \tilde{v} + k_3 \tilde{u} \tilde{v} + k_4 q)(1 - q), \quad (3)$$

with the non-negative initial condition. Here,  $q = 0$  signifies healthy, i.e., neurons are properly functioning, and  $q = 1$  implies unhealthy or no longer functioning. In studying neurodegenerative diseases, the development of coupled dynamic models plays a critical role. Different aspects of such coupled models, including those at the neuron-glia level and the amyloid-beta dynamics accounting for astrocytes, have been studied in recent papers [37, 61, 62, 63, 64, 65]. The present work is a new step in further refining such coupled models where the Markovian assumption, which cannot be justified in the general dynamic studies of neurodegenerative diseases, is removed. Before proceeding to the analysis of such refined models, we note that such models degenerate into the Markovian case once in the neural damage equation presented above, the fractional derivative  $D_t^\alpha q$  is replaced by the ordinary derivative  $dq/dt$  [43, 45].



### 3. Analysis of the Homogeneous System

Here, we analyze the temporal dynamics of the non-fractional and fractional models. First, we describe the equilibrium points of the non-fractional model (1) and their stability behaviours. The equilibrium points of the system (1) are the time-independent solutions of (1). These can be obtained by solving the system (1) with the vanishing time derivatives. Depending on the parameter values, the system (1) has many equilibrium points, and we calculate these numerically later on. Moreover, the stability of an equilibrium point depends on the nature of all eigenvalues of the Jacobian matrix evaluated at that point. The Jacobian matrix of the system (1) evaluated at an equilibrium point  $E_* = (u_*, \tilde{u}_*, v_*, \tilde{v}_*, w_*)$  is given by

$$\mathbf{J}_* = \begin{pmatrix} a_{11} & a_{12} & 0 & 0 & 0 \\ a_{21} & a_{22} & 0 & 0 & a_{25} \\ 0 & a_{32} & a_{33} & a_{34} & 0 \\ 0 & a_{42} & a_{43} & a_{44} & 0 \\ 0 & 0 & 0 & 0 & a_{55} \end{pmatrix},$$

where  $a_{11} = a_0 - 2a_1u_* - a_2\tilde{u}_*$ ,  $a_{12} = -a_2u_*$ ,  $a_{21} = a_2\tilde{u}_*$ ,  $a_{22} = -\tilde{a}_1 + a_2u_* - \mu(w_* - 2\tilde{u}_*)$ ,  $a_{25} = -\mu\tilde{u}_*$ ,  $a_{32} = -b_3v_*\tilde{v}_*$ ,  $a_{33} = b_0 - 2b_1v_* - b_2\tilde{v}_* - b_3\tilde{u}_*\tilde{v}_*$ ,  $a_{34} = -b_2v_* - b_3\tilde{u}_*v_*$ ,  $a_{42} = b_3v_*\tilde{v}_*$ ,  $a_{43} = b_2\tilde{v}_* + b_3\tilde{u}_*\tilde{v}_*$ ,  $a_{44} = -b_1 + b_2v_* + b_3\tilde{u}_*v_*$ , and  $a_{55} = c_0 - 2w_*/c_1$ . For the non-fractional model, if real parts of all the eigenvalues of  $\mathbf{J}_*$  are negative, then the equilibrium point  $E_*$  is stable; otherwise, it is unstable. The non-fractional damage equation has only one equilibrium point  $q_* = 1$ , which is stable. The equilibrium points for the non-fractional model are also the equilibrium points for the fractional model, but their stability behaviours are not the same for both models. For a fixed  $\alpha$ , an equilibrium point  $E_*$  of the fractional model is stable if all the eigenvalues  $\lambda_i$  ( $i = 1, \dots, 5$ ) of the Jacobian matrix  $\mathbf{J}_*$  satisfy  $|\arg(\lambda_i)| > \alpha\pi/2$ ; otherwise, it is unstable [56].

### 4. Network Model for the Brain Connectome

Before going to the brain connectome network model, we extend the temporal model (2) into the reaction-diffusion model in a subset of the Euclidean space. This spatial extension is crucial in understanding the spatiotemporal evolution of  $A\beta$  and  $\tau P$  in the brain connectome. Indeed, several in vitro and in vivo studies showed that the tau protein aggregates and can propagate along synapsis [66]. A spatio-temporal extension of the fractional model (2) in a general continuous spatial domain  $\Omega \subset \mathbb{R}^3$  is given by

$$D_t^\alpha u = \nabla \cdot (\mathbf{D}_1 \nabla u) + u(a_0 - a_1 u) - a_2 u \tilde{u}, \quad (4a)$$

$$D_t^\alpha \tilde{u} = \nabla \cdot (\tilde{\mathbf{D}}_1 \nabla \tilde{u}) - \tilde{a}_1 \tilde{u} + a_2 u \tilde{u} - \mu \tilde{u} (w - \tilde{u}), \quad (4b)$$

$$D_t^\alpha v = \nabla \cdot (\mathbf{D}_2 \nabla v) + v(b_0 - b_1 v) - b_2 v \tilde{v} - b_3 \tilde{u} v \tilde{v}, \quad (4c)$$

$$D_t^\alpha \tilde{v} = \nabla \cdot (\tilde{\mathbf{D}}_2 \nabla \tilde{v}) - \tilde{b}_1 \tilde{v} + b_2 v \tilde{v} + b_3 \tilde{u} v \tilde{v}, \quad (4d)$$

$$D_t^\alpha w = w(c_0 - w/c_1), \quad (4e)$$

where the first term on the right-hand side in each of the first four equations incorporates the random movement of the concentrations in the domain  $\Omega$ . We assume that the astrocytes' density remains homogeneous in the domain  $\Omega$ . Here,  $\mathbf{D}_1$ ,  $\tilde{\mathbf{D}}_1$ ,  $\mathbf{D}_2$ , and  $\tilde{\mathbf{D}}_2$  are the diffusion tensors that characterize the spreading of each protein. We consider the same damage equation (3) in this spatial extension, and hereafter, the damage

$q$  also depends on the spatial location, i.e.,  $q(\mathbf{x}, t)$ ,  $\mathbf{x} \in \Omega$ . The astrocytes also affect the damage dynamics of the neurons, as they are implicitly involved through toxic amyloid beta.

The main goal is to study the disease progression in the brain connectome. The modified model (4) is defined in a continuous domain  $\Omega$ . Therefore, we formulate the network mathematical model corresponding to the modified model (4) so that we can integrate the brain connectome data [43, 45]. Suppose the network brain data is represented by a graph  $\mathbf{G}$  with  $V$  nodes and  $E$  edges. For the graph  $\mathbf{G}$ , we construct the adjacency matrix  $\mathbf{A}$ . This helps us to construct the Laplacian in the graph. We define the  $(i, j)$  ( $i, j = 1, 2, 3, \dots, N$ ) element of the matrix  $\mathbf{A}$  as

$$A_{ij} = \frac{n_{ij}}{l_{ij}^2},$$

where  $n_{ij}$  is the mean fiber number and  $l_{ij}^2$  is the mean length squared between the nodes  $i$  and  $j$ . Now, we define the elements of the Laplacian matrix  $\mathbf{L}$  as

$$L_{ij} = \rho(D_{ij} - A_{ij}), \quad i, j = 1, 2, 3, \dots, N,$$

where  $\rho$  is the diffusion coefficient and  $D_{ii} = \sum_{j=1}^N A_{ij}$  are the elements of the diagonal weighted-degree matrix. With the help of the Laplacian matrix, we derive a network mathematical model on the graph  $\mathbf{G}$ , whose dynamics at each node  $j$  ( $j = 1, 2, 3, \dots, N$ ) are given by

$$D_t^\alpha u_j = - \sum_{k=1}^N L_{jk}^u u_j + u_j(a_0 - a_1 u_j) - a_2 u_j \tilde{u}_j, \quad (5a)$$

$$D_t^\alpha \tilde{u}_j = - \sum_{k=1}^N L_{jk}^{\tilde{u}} \tilde{u}_j - \tilde{a}_1 \tilde{u}_j + a_2 u_j \tilde{u}_j - \mu \tilde{u}_j (w_j - \tilde{u}_j), \quad (5b)$$

$$D_t^\alpha v_j = - \sum_{k=1}^N L_{jk}^v v_j + v_j(b_0 - b_1 v_j) - b_2 v_j \tilde{v}_j - b_3 \tilde{u}_j v_j \tilde{v}_j, \quad (5c)$$

$$D_t^\alpha \tilde{v}_j = - \sum_{k=1}^N L_{jk}^{\tilde{v}} \tilde{v}_j - \tilde{b}_1 \tilde{v}_j + b_2 v_j \tilde{v}_j + b_3 \tilde{u}_j v_j \tilde{v}_j, \quad (5d)$$

$$D_t^\alpha w_j = w_j(c_0 - w_j/c_1), \quad (5e)$$

and the corresponding damage equation is given by the corresponding fractional differential equation

$$D_t^\alpha q_j = (k_1 \tilde{u}_j + k_2 \tilde{v}_j + k_3 \tilde{u}_j \tilde{v}_j + k_4 q_j)(1 - q_j), \quad (6)$$

with non-negative initial conditions. Here, the homogeneous system's equilibrium points are the homogeneous stationary steady-states for the network model (5). We find these non-homogeneous stationary steady-states numerically in the next section.

## 5. Results and Discussions

This section focuses on the numerical findings for both models (non-fractional and fractional) in the brain connectome. We collect the brain connectome data from BrainGraph.org – the network of the brain (<https://braingraph.org>). These data provide information on a network containing nodes and edges in different brain regions. It helps us in studying the spatio-temporal behaviour in the brain. In these brain graph

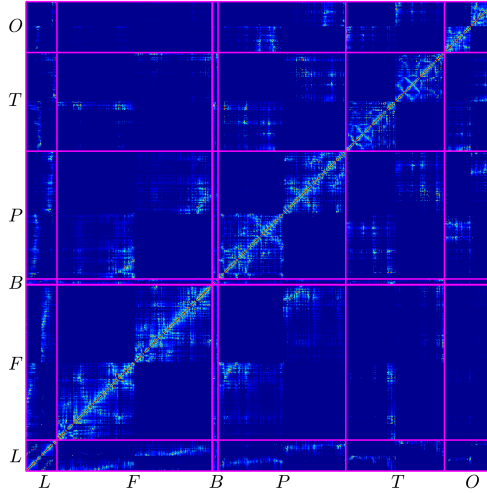


Figure 1: (Color online) Weighted adjacency matrix for the brain connectome data: limbic ( $L$ ), frontal ( $F$ ), basal ganglia ( $B$ ), parietal ( $P$ ), temporal ( $T$ ) and occipital ( $O$ ). In our integrated brain connectome data, each region contains one or more brain IDs, and they are listed in Table 1.

data, each node corresponds to a small area ( $1-1.5\text{cm}^2$ ) of the gray matter, called the region of interest (ROI). An edge may be connected with two nodes if a diffusion-MRI-based workflow finds fibers of axons running between those two nodes in the white matter of the brain [67, 68].

Regarding the computations, we have integrated the brain connectome data into our computational environment (Matlab) and exported the Laplacian corresponding to the real data. The considered network data contains  $N = 1,015$  nodes and  $V = 16,280$  edges. The mean fiber number  $n_{ij}$  in the integrated data ranges from 1 to 4966.5, with an average of 39.33 fibers per edge, with the majority of fibers located between the superior parietal and precuneus areas. In addition, the average fiber length  $l_{ij}$ , which ranges from 10.270 mm to 83.003 mm, is 30.089 mm. We use the Laplacian to find the network model's numerical solution for handling different scenarios, as considered later in this section. The Runge-Kutta method of order four has been used to integrate the resulting system with  $dt = 0.01$ , and the obtained results are unaltered for lesser values of this time step. We computed the numerical results based on our code implemented in C-language. We used Sharcnet ([www.sharcnet.ca](http://www.sharcnet.ca)) supercomputers to run multiple jobs simultaneously, which helped us efficiently analyse different aspects of the model.

Figure 1 depicts the weighted adjacency matrix for the considered network data. In the plot, blue to red colors represent the minimum to the maximum strength of the connection between the nodes. The brain stem region is also in the diagram between the frontal and basal ganglia, but it is not visible because it contains only one node. This diagram shows the connection between the nodes and regions in the brain connectome. We use this matrix to find the spatio-temporal behaviour for the network model of the brain connectome. Depending on the parameter values, both models (non-fractional and fractional models) share the feasible homogeneous steady-states. In the homogeneous steady-state, the concentration corresponding to the toxic amyloid-beta may depend on the toxic tau protein concentration. In this case, it is called secondary tauopathy; otherwise, it is a primary tauopathy. We will discuss both cases in the coming subsection.

Before moving to the numerical simulations, we first mention the initial conditions for the variables in

Table 1: Brain IDs associated with brain regions [69].

Brain region	Brain ID
Limbic	Rostralanteriorcingulate, Posteriorcingulate, Caudalanteriorcingulate, Parahippocampal, Isthmuscingulate, Entorhinal
Frontal	Lateralorbitofrontal, Parsorbitalis, Frontalpole, Medialorbitofrontal, Parstriangularis, Parsopercularis, Precentral, Rostralmiddlefrontal, Superiorfrontal, Caudalmiddlefrontal
Parietal	Postcentral, Supramarginal, Superiorparietal, Inferiorparietal, Precuneus, Paracentral
Basal Ganglia	Right-Thalamus-Proper, Right-Caudate, Right-Putamen, Right-Pallidum, Right-Accumbens-area, Right-Amygdala, Left-Thalamus-Proper, Left-Caudate, Left-Putamen, Left-Pallidum, Left-Accumbens-area, Left-Amygdala
Brain Stem	Brain-Stem
Occipital	Cuneus, Pericalcarine, Lateraloccipital, Lingual
Temporal	Left-Hippocampus, Right-Hippocampus, Temporalpole, Inferiortemporal, Middletemporal, Bankssts, Superiortemporal, Transversetemporal, Insula, Fusiform

the network model. In the brain connectome, the initial seeding sites for the toxic amyloid-beta are the temporobasal and frontomedial regions, and the toxic tau proteins are the locus coeruleus and transentorhinal associated regions. These seeding sites in the brain connectome are mentioned in [43, 45]. Here, we add small toxic loads 0.25% and 0.38% in the toxic amyloid-beta ( $\tilde{u}$ ) and toxic tau protein ( $\tilde{v}$ ) concentrations for the seeding sites, respectively. Due to these small perturbations, the toxic concentrations propagate all over the brain connectome and spread AD. On the other hand, we consider healthy concentrations for both amyloid-beta ( $u$ ) and tau proteins ( $v$ ) and a small concentration for the astrocytes ( $w$ ). Some other perturbations of these initial concentrations can change the initial propagation profiles of the concentrations, but the final results (long-term behaviours) are the same. These concentrations are uniform on all the nodes in the brain connectome. We consider the initial condition  $q = 0$  for all the nodes for the damage equation. As toxic loads propagate over the brain connectome, they damage the neurons in the brain.

### 5.1. Primary and secondary tauopathies

As in our previous study, we have shown that the evolution profiles of both toxic loads remain the same for primary and secondary tauopathies in the absence of memory ( $\alpha = 1$ ) and astrocytes [45]. Here also, we observe that their profiles remain the same for both tauopathies in the presence of astrocytes. So, without the loss of generality, we present the results for the parameter values corresponding to the secondary tauopathy. Table 2 mentions a synthetic parameter set for the secondary tauopathy. For this parameter set, the non-trivial equilibrium point  $E_* = (0.596, 0.154, 0.33, 0.14, 0.1)$  is locally asymptotically stable, and a numerical solution of the system is shown in Fig. 2. We also studied a more general case (mixed tauopathy) where non-uniform parameter values are considered on different nodes in the brain connectome.

#### 5.1.1. Dual role of astrocytes

As we stated earlier, the astrocytes play a dual role in disease propagation. Astrocytes try to clear the toxic amyloid-beta and maintain a healthy balance in the brain. However, due to the accumulation of high concentrations of toxic amyloid-beta, astrocytes over-activate and help propagate the disease rather than save the brain from the disease. Therefore, two scenarios can occur depending on the concentrations of astrocytes present in the brain cells: (i) astrocytes control the toxic amyloid-beta, and (ii) astrocytes can not control the toxic amyloid-beta. Here, we capture both cases through our considered network mathematical model in the absence of memory. In our model, the parameter  $c_1$  represents the brain cells' maximum

Table 2: Synthetic parameter values [43].

Parameter	Value	Parameter	Value	Parameter	Value
$a_0$	1.035	$a_1$	1.38	$a_2$	1.38
$\tilde{a}_1$	0.828	$b_0$	0.69	$b_1$	1.38
$b_2$	1.035	$\tilde{b}_1$	0.552	$b_3$	4.14
$c_0$	1.0	$c_1$	0.1	$\mu$	0.1
$\rho_1$	1.38	$\rho_2$	0.138	$\rho_3$	1.38
$\rho_4$	0.014	$k_1$	0.0001	$k_2$	0.01
$k_3$	0.1	$k_4$	0.001		

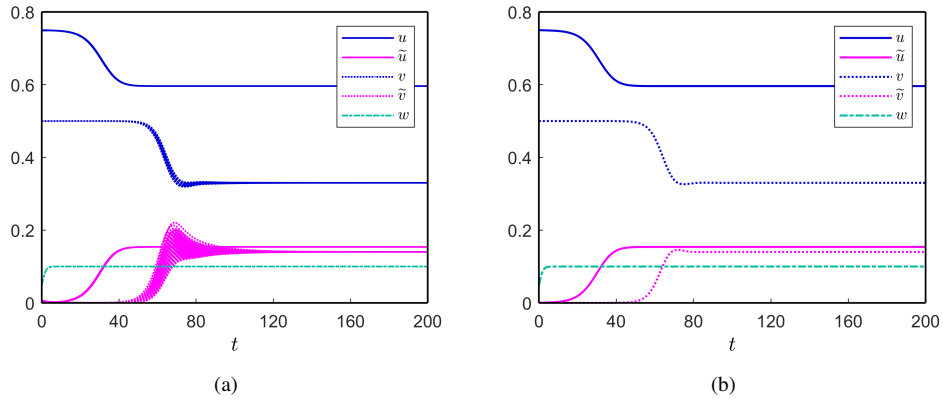


Figure 2: (Color online) Solutions for the non-fractional model of (5) in the brain connectome: (a) solutions in each region and (b) the spatial average solution. The parameter values are in Table 2.

concentration (carrying capacity) of astrocytes. We consider two different carrying capacities for the astrocytes in the network model, and the average toxic density propagations over time are shown in Fig. 3. For  $c_1 = 0.3$ , with an increase in the clearance rate  $\mu$ , the toxic load over the brain connectome decreases [see Fig. 3(a)]. This shows that astrocytes can control the brain's toxic loads. On the other hand, for  $c_1 = 0.1$ , they fail to control the healthy balance in the brain connectome and support an increase in the toxic loads [see Fig. 3(b)]. In both cases, the non-trivial equilibrium point  $E_*$  is locally asymptotically stable.

### 5.1.2. Memory effect

Once memory effects become significant, the Markovian framework does not adequately describe the underlying complex dynamic processes behind the development and progression of neurodegenerative diseases. Here, we analyze the memory effect of AD progression in the brain connectome. As mentioned earlier, the model (5) has a memory for  $0 < \alpha < 1$  and memoryless for  $\alpha \rightarrow 1$ . As discussed in Sect 2, the underlying processes are non-Markovian. Figure 4 depicts both the toxic propagation over the brain connectome for no-memory and with memory. In the figure, we plot the spatial average of toxic amyloid-beta and toxic tau protein. In both cases ( $\alpha = 0.9$  and  $\alpha = 0.8$ ), the non-trivial equilibrium point  $E_*$  satisfies the conditions for locally asymptotically stable, as mentioned in Sect 3. Here, the evolution time of the toxic loads for the fractional model is higher compared to the non-fractional model. Furthermore, with an

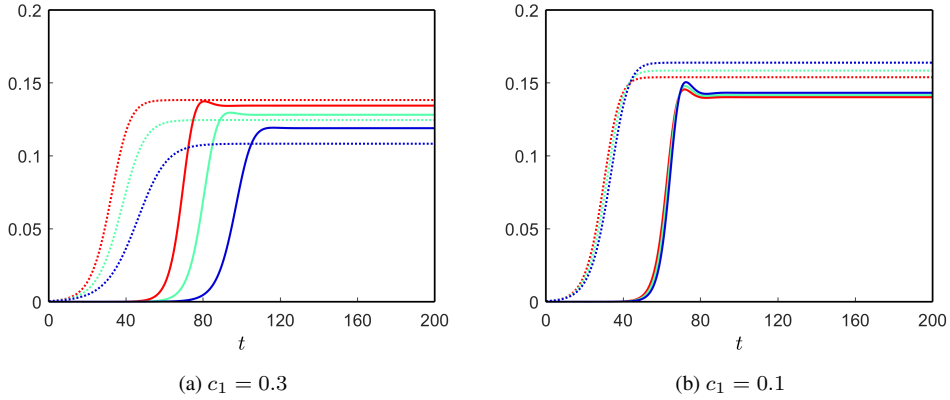


Figure 3: (Color online) Spatial average solutions of  $\tilde{u}$  (dotted) and  $\tilde{v}$  (solid) for the non-fractional model (5) for different values of  $c_1$  and  $\mu$ :  $\mu = 0.1$  (red),  $\mu = 0.2$  (green) and  $\mu = 0.3$  (blue). The other parameter values are in Table 2.

increase in the memory effect (decreasing the value of  $\alpha$ ), the evolution time of toxic loads also increases [see Fig. 4].

### 5.1.3. Neuronal damage

Following the model (6), the neuronal damage depends on the toxic loads in the brain connectome; hence, the requirement depends on the evolutionary time (the time required to converge to the stable steady-state) of toxic loads. We mention the parameter values directly associated with the neuronal damage in Table 2. These parameter values give us the influence of toxic tau proteins on neural damage and also in the presence of toxic amyloid-beta [70, 71, 72, 73]. We plot the spatial average of the damage in Fig. 4, and it validates the dependency. It has been observed that the damage converges to its equilibrium point  $q_* = 1$  for both fractional and non-fractional models, but the case of the fractional model takes a longer time than the non-fractional model. Overall, memory has a pronounced effect on AD propagation.

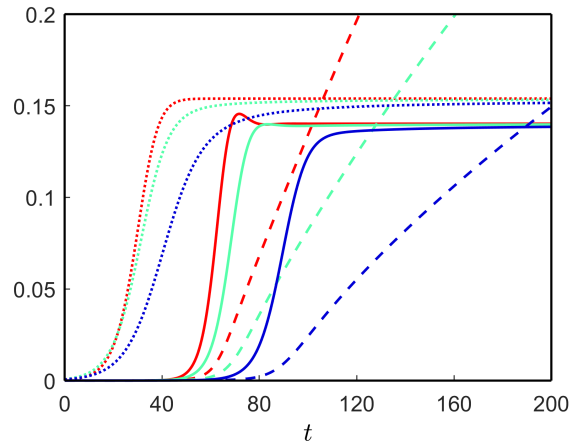


Figure 4: (Color online) Spatial average solutions of  $\tilde{u}$  (dotted),  $\tilde{v}$  (solid) and  $q$  (dashed) for the fractional model of (5) with (6) for different values of  $\alpha$  with the other fixed parameter values of Table 2 over the brain connectome. In the plot  $\alpha = 1$ ,  $\alpha = 0.9$  and  $\alpha = 0.8$  are represented by the red, green and blue curves, respectively.



## 5.2. Mixed tauopathy

Here, we focus on disease propagation for non-uniform parameters over the brain connectome. This is more realistic than the uniform parameters as the presence of heterogeneous density of the ingredients in the brain (e.g., proteins, chemical ions, etc.). We consider the parameter values of  $b_2$  and  $b_3$  from Table 2 in all the brain identities (IDs) except some regions mentioned in Tables 3 and 4. The methodology of getting these values is mentioned in [43]. Due to the non-uniform parameter values in the brain connectome, a mixture of primary and secondary tauopathies, called mixed tauopathy, occurs in the network model. This causes different stable coexisting steady-states in the network model, and we divide these into two parts: region ID and region-wise disease propagation.

Table 3: Modified  $b_2$  and  $b_3$  parameter values in different brain IDs [43].

Brain ID	$b_2$	$b_3$
Entorhinal cortex	3.125	1.104e-5
Pallidum	2.76	2.76
Locus coeruleus	1.38	1.38
Putamen	3.795	3.795
Precuneus	3.105	3.105

### 5.2.1. Region ID-wise AD propagation

The integrated brain connectome data has forty-nine brain IDs, each containing one or more nodes. We calculate the average concentration of the toxic amyloid-beta for each brain ID by the formula [69]:

$$M_{\tilde{u}}^d = \frac{1}{n_d} \sum_{k \in \mathcal{R}_d} \tilde{u}_k, \quad (7)$$

where  $\mathcal{R}_d$  is defined as the set of all nodes in that brain ID, and  $n_d$  is the number of elements in  $\mathcal{R}_d$ . We use the same formula for the toxic tau proteins and also for the damage dynamics. For the non-fractional model, we observe uniform average concentrations of toxic amyloid-beta (not shown here) and non-uniform average concentrations of toxic tau proteins along the brain IDs [see Fig. 5 (a)]. This happens due to the direct involvement of the non-uniform parameters  $b_2$  and  $b_3$  in the healthy and toxic tau proteins equations. Furthermore, the damage propagation profiles for each brain ID are different [see Fig. 5 (b)]. According to the integrated brain connectome data, the maximum concentrations of toxic amyloid-beta accumulate in the region ID precuneus, followed by the region IDs left-putamen, right-putamen, entorhinal, and so on. The damage dynamics show that these region IDs affect the most at the initial stage of AD progression.

### 5.2.2. Region-wise AD propagation

Now, we focus on the evolution of the toxic load distributions and their damage profile for seven brain regions (limbic, frontal, basal ganglia, parietal, temporal, occipital, and brain stem), and each region containing one or more brain IDs. The integrated brain connectome data contains Cartesian coordinates for all the nodes in three-dimensional space and their brain IDs. We plot them according to their regions (mentioned in Table 1) in Fig. 6, and in the plot, different colors of the nodes belong to different regions. We have used the same color codes in Figs. 6 and 7 for the brain regions.

Table 4: Modified  $b_3$  parameter values in different brain IDs [43].

Brain ID and modified $b_3$ value			
Pars opercularis	7.452	Rostral middle frontal gyrus	6.707
Superior frontal gyrus	7.452	Caudal middle frontal gyrus	7.452
Precentral gyrus	5.589	Postcentral gyrus	3.726
Lateral orbitofrontal cortex	6.486	Medial orbitofrontal cortex	6.486
Pars triangularis	5.520e-6	Rostral anterior cingulate	6.210e-6
Posterior cingulate cortex	3.45	Inferior temporal cortex	13.11
Middle temporal gyrus	11.04	Superior temporal sulcus	8.97
Superior temporal gyrus	8.28	Superior parietal lobule	12.42
Cuneus	13.8	Pericalcarine cortex	13.8
Inferior parietal lobule	11.73	Lateral occipital sulcus	15.18
Lingual gyrus	13.8	Fusiform gyrus	7.59
Parahippocampal gyrus	11.04	Temporal pole	1.104e-5

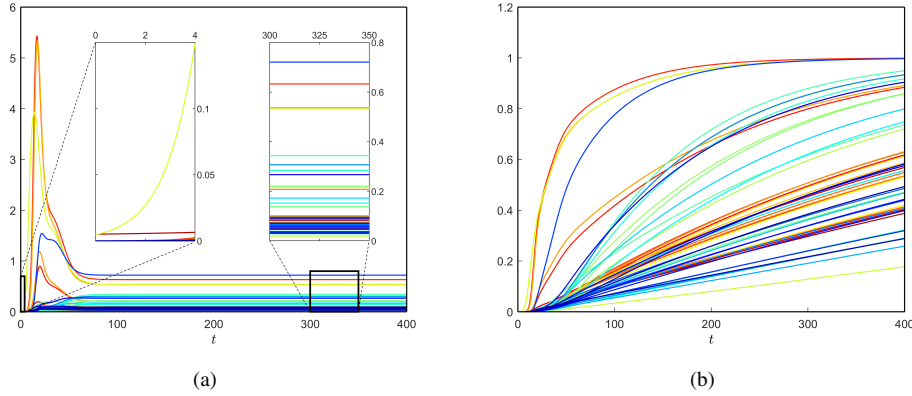


Figure 5: (Color online) Brain ID-wise average toxic tau protein ( $\tilde{v}$ ) propagation (a) and the corresponding neural damage (b) for the non-fractional model. Here, we choose the fixed parameter values  $\mu = 0.2$ ,  $c_1 = 0.3$  and others from Table 2 for all the brain connectome nodes except those listed in Tables 3 and 4.

We apply the formula (7) to find the average toxic loads for all regions. In this case, the summation is taken over the nodes belonging to the respective regions. We plot the toxic load corresponding to the tau protein for each region in Fig. 7. Due to the non-uniform parameter set in the tau protein equation, the toxic load converges to different concentrations over the regions. According to the integrated data, the occipital region accumulates the most toxic concentration, followed by the parietal, basal ganglia, limbic, temporal, frontal, and brain stem. Moreover, the toxic propagation profile for each region is different. Some regions accumulate more toxic tau protein concentration after the initial development of the disease but settle down to a comparatively lower concentration for a longer time, e.g., basal ganglia, parietal, and limbic. For the other regions, there is not much accumulation in the concentration after the start of the disease; rather, they slowly accumulate the toxic loads and help in disease propagation. Figures 7(a) and (b) represent the toxic tau protein propagation in regions for the non-fractional model and fractional model with  $\alpha = 0.8$ ,

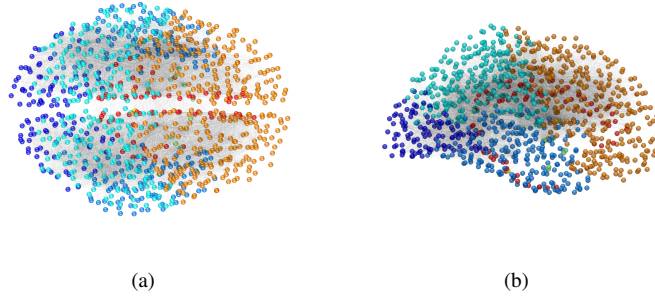


Figure 6: (Color online) Three-dimensional views of the positions of the nodes for the integrated brain connectome data: (a) axial view and (b) sagittal view. Different colors are used to indicate different brain regions.

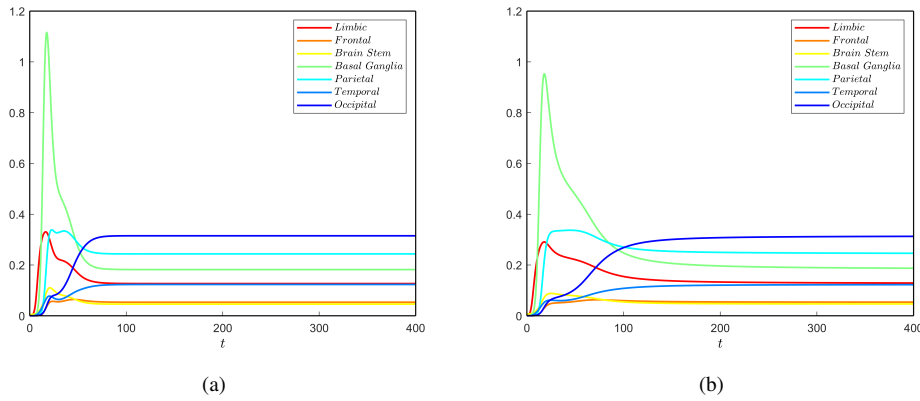


Figure 7: (Color online) Brain region-wise average toxic tau protein ( $\bar{v}$ ) propagation: (a) non-fractional model and (b) fractional model with  $\alpha = 0.8$ . Here, we choose the fixed parameter values  $\mu = 0.2$ ,  $c_1 = 0.3$  and others from Table 2 for all the nodes in the brain connectome except the nodes listed in Tables 3 and 4.

respectively (other parameters are mentioned in the caption and Tables 2, 3 and 4). This comparison shows that the memory effect helps in slowing down the propagation speed in the brain regions. We have observed the fractional model for other values of  $\alpha (< 1)$ , and the propagation speed decreases with decreasing values of  $\alpha$ .

We apply the same formula (7) to find the regions' average damage profile. The damage profile for each region is different due to the non-uniform distributions of the toxic tau proteins. The region corresponding to the maximum toxic concentration is damaged first, then the region with the second-highest concentration, and so on. Figure 8 shows the node-wise neuronal damage propagation for both non-fractional and fractional models. In the results, the damage dynamics are shown till  $t = 400$  (non-dimensional time), but we observe that the required time to damage each region in the brain for the fractional model is higher than the non-fractional model. Hence, the memory effect takes longer to damage the brain cells.

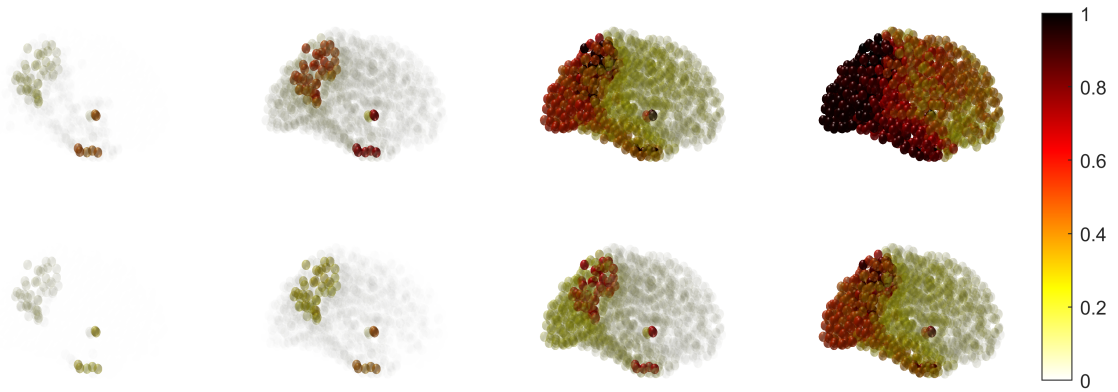


Figure 8: (Color online) Node-wise damage propagation for the non-fractional model (upper panel) and fractional ( $\alpha = 0.8$ ) model (lower panel) in brain connectome. We choose the fixed parameter values  $\mu = 0.2$ ,  $c_1 = 0.3$  and Table 2 for all the nodes in the brain connectome except the nodes listed in Tables 3 and 4. The dark red represents the high damage, and the light yellow represents the low damage.

## 6. Summary

In this work, we have considered a modified heterodimer model for protein-protein interactions for each of the proteins ( $A\beta$  and  $\tau P$ ), accounting for their coupling. We incorporated the coupled dynamics of astrocytes dynamics into the modified model and studied the dual role of astroglia before and after AD. Furthermore, we have studied the memory effect in AD progression, which is highly relevant to disease progression. Most of these investigations have been carried out by considering the heterogeneous parameter values, and it is a more realistic synthetic parameter set-up.

Depending on the presence of astrocytes, the considered network model shows a dual behaviour in disease propagation. For higher astrocyte density, the density corresponding to the toxic amyloid-beta increases with an increase in its clearance rate by astrocytes. On the other hand, for smaller astrocyte densities, the opposite scenario holds. Therefore, if sufficient astrocytes are present in the brain, they can minimize or delay AD development; otherwise, they help in AD propagation. Furthermore, the fractional differential derivative framework presented here helps to model the memory effect on AD progression. We have shown that an increase in memory (by decreasing the parameter values  $\alpha$ ) causes a delay in the toxic density propagations in the brain. As a result, it slows down AD development in the brain, giving experimentalists more freedom in terms of parameters to fit their data appropriately.

We have studied the network model for the parameter values where primary and secondary tauopathies conditions are satisfied in different brain regions. This causes a non-homogeneous distribution of toxic tau proteins in the brain. In addition, the network model shows that highly connected nodes are more likely to become infected and turn into disease distribution hubs. Furthermore, different neuronal damage profiles are shown on different brain IDs and in different brain regions. Hence, heterogeneous parameter values in the network model capture a realistic scenario of AD progression in the brain [74]. These non-uniform parameter values in the parameters involved in the amyloid-beta could be a good extension of this work. The coupling of astrocytes to  $A\beta$  and  $\tau P$  represents an advancement in this direction, and one could use this model in an experimental set-up for better data fitting. Along with the memory, considering heterogeneous parameter values corresponding to amyloid-beta or astrocytes in different brain IDs or regions is an important avenue for future research on this model. To a greater extent, neurodegenerative diseases involve

complex and multiscale processes with multiple levels of biological framework, ranging from molecular and cellular to systemic and even societal. The presented work and the developed methodology allow us to reveal new trends and additional features of the underlying processes. More refined views on the complex dynamics of neurodegenerative diseases are expected with the subsequent incorporation of other scales (e.g., molecular-to-cellular, macro-to-micro) into the coupled biological framework.

## Acknowledgements

The authors are grateful to the NSERC and the CRC Program for their support. RM also acknowledges the support of the BERC 2022–2025 program and the Spanish Ministry of Science, Innovation and Universities through the Agencia Estatal de Investigacion (AEI) BCAM Severo Ochoa excellence accreditation SEV-2017–0718 and the Basque Government fund AI in BCAM EXP. 2019/00432. This research was enabled in part by support provided by SHARCNET ([www.sharcnet.ca](http://www.sharcnet.ca)) and Digital Research Alliance of Canada ([www.alliancecan.ca](http://www.alliancecan.ca)).

## References

- [1] A. Alzheimer, Über einen eigenartigen schweren erkrankungsprozeß der hirnrinde., *Neurol Central*. 25 (1906) 1134.
- [2] H. Möller, M. Graeber, The case described by Alois Alzheimer 1911, *Eur. Arch Psychiatry Clin Neurosci*. 248 (1998) 111–127.
- [3] H. Hippus, G. Neundörfer, The discovery of Alzheimer’s disease, *Dialogues Clin Neurosci*. 5 (2003) 101–108.
- [4] D. Harman, Alzheimer’s disease pathogenesis: role of aging, *Annals of the New York Academy of Sciences* 1067 (1) (2006) 454–460.
- [5] R. Sengoku, Aging and Alzheimer’s disease pathology, *Neuropathology* 40 (1) (2020) 22–29.
- [6] E. Bagyinszky, Y. C. Youn, S. S. A. An, S. Kim, The genetics of Alzheimer’s disease, *Clinical interventions in aging* 9 (2014) 535.
- [7] G. T. Grossberg, Diagnosis and treatment of Alzheimer’s disease, *Journal of Clinical Psychiatry* 64 (2003) 3–6.
- [8] M. F. Weiner, L. Hyman, M. Bret, C. White Iii, Early behavioral symptoms and course of Alzheimer’s disease, *Acta Psychiatrica Scandinavica* 111 (5) (2005) 367–371.
- [9] J. Sevigny, P. Chiao, T. Bussière, P. H. Weinreb, L. Williams, M. Maier, R. Dunstan, S. Salloway, T. Chen, Y. Ling, et al., The antibody aducanumab reduces A $\beta$  plaques in Alzheimer’s disease, *Nature* 537 (7618) (2016) 50–56.
- [10] D. J. Selkoe, Alzheimer disease and aducanumab: adjusting our approach, *Nature Reviews Neurology* 15 (7) (2019) 365–366.
- [11] R. Howard, K. Y. Liu, Questions emerge as biogen claims aducanumab turnaround, *Nature Reviews Neurology* 16 (2) (2020) 63–64.
- [12] M. Murphy, H. LeVine III, Alzheimer’s disease and the  $\beta$ -amyloid peptide, *J Alzheimers Dis* 19 (1) (2010) 311–323.
- [13] G. K. Gouras, T. T. Olsson, O. Hansson,  $\beta$ -amyloid peptides and amyloid plaques in Alzheimer’s disease, *Neurotherapeutics* 12 (1) (2015) 3–11.
- [14] C. Liu, The role of mesenchymal stem cells in regulating astrocytes-related synapse dysfunction in early Alzheimer’s disease, *Frontiers in Neuroscience* 16 (2022) 927256.
- [15] E. B. Rischel, M. Gejl, B. Brock, J. Rungby, A. Gjedde, In Alzheimer’s disease, amyloid beta accumulation is a protective mechanism that ultimately fails, *Alzheimer’s & dementia: the journal of the Alzheimer’s Association* (2022).
- [16] A. R. Roda, G. Serra-Mir, L. Montoliu-Gaya, L. Tiessler, S. Villegas, Amyloid-beta peptide and tau protein crosstalk in Alzheimer’s disease, *Neural Regeneration Research* 17 (8) (2022) 1666.
- [17] X. Sun, W.-D. Chen, Y.-D. Wang,  $\beta$ -amyloid: the key peptide in the pathogenesis of Alzheimer’s disease, *Frontiers in pharmacology* 6 (2015) 221.
- [18] D. Burdick, B. Soreghan, M. Kwon, J. Kosmoski, M. Knauer, A. Henschen, J. Yates, C. Cotman, C. Glabe, Assembly and aggregation properties of synthetic Alzheimer’s A4/beta amyloid peptide analogs, *Journal of Biological Chemistry* 267 (1) (1992) 546–554.
- [19] S. A. Gravina, L. Ho, C. B. Eckman, K. E. Long, L. Otvos, L. H. Younkin, N. Suzuki, S. G. Younkin, Amyloid  $\beta$  protein ( $a\beta$ ) in Alzheimer’s disease brain: Biochemical and immunocytochemical analysis with antibodies specific for forms ending at  $a\beta$ 40 or  $a\beta$ 42, *Journal of Biological Chemistry* 270 (13) (1995) 7013–7016.
- [20] J. Kim, L. Onstead, S. Randle, R. Price, L. Smithson, C. Zwizinski, D. W. Dickson, T. Golde, E. McGowan, A $\beta$ 40 inhibits amyloid deposition in vivo, *Journal of Neuroscience* 27 (3) (2007) 627–633.

- [21] R. Medeiros, D. Baglietto-Vargas, F. M. LaFerla, The role of tau in Alzheimer's disease and related disorders, *CNS neuroscience & therapeutics* 17 (5) (2011) 514–524.
- [22] S. Muralidar, S. V. Ambi, S. Sekaran, D. Thirumalai, B. Palaniappan, Role of tau protein in Alzheimer's disease: The prime pathological player, *International journal of biological macromolecules* 163 (2020) 1599–1617.
- [23] T. Guo, W. Noble, D. P. Hanger, Roles of tau protein in health and disease, *Acta neuropathologica* 133 (5) (2017) 665–704.
- [24] R. B. Kargbo, Treatment of Alzheimer's by PROTAC-Tau protein degradation (2019).
- [25] S. Illenberger, Q. Zheng-Fischhofer, U. Preuss, K. Stamer, K. Baumann, B. Trinczek, J. Biernat, R. Godemann, E.-M. Mandelkow, E. Mandelkow, The endogenous and cell cycle-dependent phosphorylation of tau protein in living cells: implications for Alzheimer's disease, *Molecular biology of the cell* 9 (6) (1998) 1495–1512.
- [26] K. A. Johnson, S. Minoshima, N. I. Bohnen, K. J. Donohoe, N. L. Foster, P. Herscovitch, J. H. Karlawish, C. C. Rowe, M. C. Carrillo, D. M. Hartley, et al., Appropriate use criteria for amyloid PET: a report of the amyloid imaging task force, the society of nuclear medicine and molecular imaging, and the Alzheimer's association, *Alzheimer's & Dementia* 9 (1) (2013) E1–E16.
- [27] M. Grundman, K. A. Johnson, M. Lu, A. Siderowf, A. K. Arora, D. M. Skovronsky, M. A. Mintun, M. J. Pontecorvo, et al., Effect of amyloid imaging on the diagnosis and management of patients with cognitive decline: impact of appropriate use criteria, *Dementia and geriatric cognitive disorders* 41 (1-2) (2016) 80–92.
- [28] G. D. Rabinovici, C. Gatsonis, C. Apgar, K. Chaudhary, I. Gareen, L. Hanna, J. Hendrix, B. E. Hillner, C. Olson, O. H. Lesman-Segev, et al., Association of amyloid positron emission tomography with subsequent change in clinical management among medicare beneficiaries with mild cognitive impairment or dementia, *Jama* 321 (13) (2019) 1286–1294.
- [29] M. D. Devous, A. D. Joshi, M. Navitsky, S. Southekal, M. J. Pontecorvo, H. Shen, M. Lu, W. R. Shankle, J. P. Seibyl, K. Marek, et al., Test-retest reproducibility for the tau PET imaging agent Flortaucipir F 18, *Journal of Nuclear Medicine* 59 (6) (2018) 937–943.
- [30] M. D. Devous Sr, A. S. Fleisher, M. J. Pontecorvo, M. Lu, A. Siderowf, M. Navitsky, I. Kennedy, S. Southekal, T. S. Harris, M. A. Mintun, Relationships between cognition and neuropathological tau in Alzheimer's disease assessed by 18F Flortaucipir PET, *Journal of Alzheimer's Disease* 80 (3) (2021) 1091–1104.
- [31] N. J. Abbott, L. Rönnbäck, E. Hansson, Astrocyte-endothelial interactions at the blood-brain barrier, *Nature reviews neuroscience* 7 (1) (2006) 41–53.
- [32] C. Eroglu, B. A. Barres, Regulation of synaptic connectivity by glia, *Nature* 468 (7321) (2010) 223–231.
- [33] K. Hayakawa, E. Esposito, X. Wang, Y. Terasaki, Y. Liu, C. Xing, X. Ji, E. H. Lo, Transfer of mitochondria from astrocytes to neurons after stroke, *Nature* 535 (7613) (2016) 551–555.
- [34] Y. Kim, J. Park, Y. K. Choi, The role of astrocytes in the central nervous system focused on bk channel and heme oxygenase metabolites: a review, *Antioxidants* 8 (5) (2019) 121.
- [35] O. E. Tasdemir-Yilmaz, M. R. Freeman, Astrocytes engage unique molecular programs to engulf pruned neuronal debris from distinct subsets of neurons, *Genes & development* 28 (1) (2014) 20–33.
- [36] S. Koizumi, Y. Hirayama, Y. M. Morizawa, New roles of reactive astrocytes in the brain; an organizer of cerebral ischemia, *Neurochemistry international* 119 (2018) 107–114.
- [37] S. Pal, R. Melnik, The role of astrocytes in Alzheimer's disease progression, in: I. Rojas, O. Valenzuela, F. Rojas, L. J. Herrera, F. Ortuño (Eds.), *Bioinformatics and Biomedical Engineering*, Springer, 2022, pp. 47–58.
- [38] M. Yuan, H. Wu, Astrocytes in the traumatic brain injury: the good and the bad, *Experimental Neurology* 348 (2022) 113943.
- [39] C. Garwood, L. Ratcliffe, J. Simpson, P. Heath, P. Ince, S. Wharton, astrocytes in Alzheimer's disease and other age-associated dementias: a supporting player with a central role, *Neuropathology and Applied Neurobiology* 43 (4) (2017) 281–298.
- [40] A. Y. Abramov, M. R. Duchon, The role of an astrocytic NADPH oxidase in the neurotoxicity of amyloid beta peptides, *Philosophical Transactions of the Royal Society B: Biological Sciences* 360 (1464) (2005) 2309–2314.
- [41] Y. S. Kim, H. M. Jung, B.-E. Yoon, Exploring glia to better understand Alzheimer's disease, *Animal cells and systems* 22 (4) (2018) 213–218.
- [42] C.-C. Liu, N. Zhao, Y. Fu, N. Wang, C. Linares, C.-W. Tsai, G. Bu, ApoE4 accelerates early seeding of amyloid pathology, *Neuron* 96 (5) (2017) 1024–1032.
- [43] T. B. Thompson, P. Chaggar, E. Kuhl, A. Goriely, A. D. N. Initiative, Protein-protein interactions in neurodegenerative diseases: A conspiracy theory, *PLoS computational biology* 16 (10) (2020) e1008267.
- [44] G. Meisl, E. Hidari, K. Allinson, T. Rittman, S. L. DeVos, J. S. Sanchez, C. K. Xu, K. E. Duff, K. A. Johnson, J. B. Rowe, et al., In vivo rate-determining steps of tau seed accumulation in Alzheimer's disease, *Science advances* 7 (44) (2021) eabh1448.
- [45] S. Pal, R. Melnik, Nonlocal models in the analysis of brain neurodegenerative protein dynamics with application to Alzheimer's disease, *Scientific Reports* 12 (1) (2022) 1–13.
- [46] M. T. Tacconi, Neuronal death: is there a role for astrocytes?, *Neurochemical research* 23 (5) (1998) 759–765.



- [47] D. R. Thal, The role of astrocytes in amyloid  $\beta$ -protein toxicity and clearance, *Experimental neurology* 236 (1) (2012) 1–5.
- [48] Y. Chen, F. Liu, Q. Yu, T. Li, Review of fractional epidemic models, *Applied mathematical modelling* 97 (2021) 281–307.
- [49] A. Stanislavsky, Memory effects and macroscopic manifestation of randomness, *Physical Review E* 61 (5) (2000) 4752.
- [50] J. Cressoni, G. Viswanathan, A. Ferreira, M. da Silva, Alzheimer random walk model: two previously overlooked diffusion regimes, *Physical Review E* 86 (4) (2012) 042101.
- [51] J. Cressoni, L. Da Silva, G. Viswanathan, M. Da Silva, Robustness of the non-Markovian Alzheimer walk under stochastic perturbation, *EPL (Europhysics Letters)* 100 (6) (2013) 60003.
- [52] M. Saeedian, M. Khalighi, N. Azimi-Tafreshi, G. Jafari, M. Ausloos, Memory effects on epidemic evolution: The susceptible-infected-recovered epidemic model, *Physical Review E* 95 (2) (2017) 022409.
- [53] M. I. Tropicovsky, S. A. Seminara, M. A. Fabio, A review on fractional differential equations and a numerical method to solve some boundary value problems, *Nonlinear Systems-Theoretical Aspects and Recent Applications* (2019).
- [54] M. Mohammad, A. Trounev, Explicit tight frames for simulating a new system of fractional nonlinear partial differential equation model of Alzheimer disease, *Results in Physics* 21 (2021) 103809.
- [55] A. R. Carvalho, C. Pinto, D. Baleanu, HIV/HCV coinfection model: a fractional-order perspective for the effect of the HIV viral load, *Advances in Difference Equations* 2018 (1) (2018) 1–22.
- [56] U. Ghosh, S. Pal, M. Banerjee, Memory effect on Bazykin’s prey-predator model: Stability and bifurcation analysis, *Chaos, Solitons & Fractals* 143 (2021) 110531.
- [57] R. Thuraisingham, A kinetic scheme to examine the role of glial cells in the pathogenesis of Alzheimer’s disease, *Metabolic Brain Disease* (2022) 1–5.
- [58] T. Frank, Strongly nonlinear stochastic processes in physics and the life sciences, *International Scholarly Research Notices* 2013 (2013).
- [59] M. Aguilera, C. L. Buckley, Recurrent, nonequilibrium systems and the markov blanket assumption (2022).
- [60] M. Caputo, Linear models of dissipation whose  $q$  is almost frequency independent—ii, *Geophysical Journal International* 13 (5) (1967) 529–539.
- [61] S. Pal, R. Melnik, Coupled neural–glial dynamics and the role of astrocytes in alzheimer’s disease, *Mathematical and Computational Applications* 27 (3) (2022) 33.
- [62] H. Shaheen, R. Melnik, S. Singh, ADNI, Data-driven stochastic model for quantifying the interplay between amyloid-beta and calcium levels in alzheimer’s disease, *arXiv preprint arXiv:2306.10373* (2023).
- [63] S. Pal, R. Melnik, Modelling of anti-amyloid-beta therapy for alzheimer’s disease, in: *International Work-Conference on Bioinformatics and Biomedical Engineering*, Springer, 2023, pp. 431–442.
- [64] H. Shaheen, S. Pal, R. Melnik, Astrocytic clearance and fragmentation of toxic proteins in alzheimer’s disease on large-scale brain networks, *Physica D: Nonlinear Phenomena* 454 (2023) 133839.
- [65] H. Shaheen, R. Melnik, ADNI, Bayesian inference and role of astrocytes in amyloid-beta dynamics with modelling of alzheimer’s disease using clinical data, *arXiv preprint arXiv:2306.12520* (2023).
- [66] S. L. DeVos, B. T. Corjuc, D. H. Oakley, C. K. Nobuhara, R. N. Bannon, A. Chase, C. Commins, J. A. Gonzalez, P. M. Dooley, M. P. Frosch, et al., Synaptic tau seeding precedes tau pathology in human alzheimer’s disease brain, *Frontiers in neuroscience* 12 (2018) 267.
- [67] C. Kerepesi, B. Szalkai, B. Varga, V. Grolmusz, How to direct the edges of the connectomes: Dynamics of the consensus connectomes and the development of the connections in the human brain, *Plos one* 11 (6) (2016) e0158680.
- [68] B. Szalkai, C. Kerepesi, B. Varga, V. Grolmusz, High-resolution directed human connectomes and the consensus connectome dynamics, *Plos one* 14 (4) (2019) e0215473.
- [69] S. Fornari, A. Schäfer, E. Kuhl, A. Goriely, Spatially-extended nucleation-aggregation-fragmentation models for the dynamics of prion-like neurodegenerative protein-spreading in the brain and its connectome, *Journal of theoretical biology* 486 (2020) 110102.
- [70] S. A. Small, K. Duff, Linking  $A\beta$  and tau in late-onset Alzheimer’s disease: a dual pathway hypothesis, *Neuron* 60 (4) (2008) 534–542.
- [71] A. Lloret, M.-C. Badia, E. Giraldo, G. Ermak, M.-D. Alonso, F. V. Pallardó, K. J. Davies, J. Viña, Amyloid- $\beta$  toxicity and tau hyperphosphorylation are linked via RCAN1 in Alzheimer’s disease, *Journal of Alzheimer’s Disease* 27 (4) (2011) 701–709.
- [72] H. Cho, J. Y. Choi, M. S. Hwang, Y. J. Kim, H. M. Lee, H. S. Lee, J. H. Lee, Y. H. Ryu, M. S. Lee, C. H. Lyoo, In vivo cortical spreading pattern of tau and amyloid in the Alzheimer disease spectrum, *Annals of neurology* 80 (2) (2016) 247–258.
- [73] C. R. Jack Jr, D. A. Bennett, K. Blennow, M. C. Carrillo, B. Dunn, S. B. Haeblerlein, D. M. Holtzman, W. Jagust, F. Jessen, J. Karlawish, et al., NIA-AA research framework: toward a biological definition of Alzheimer’s disease, *Alzheimer’s & Dementia* 14 (4) (2018) 535–562.
- [74] P. S. Insel, E. C. Mormino, P. S. Aisen, W. K. Thompson, M. C. Donohue, Neuroanatomical spread of amyloid  $\beta$  and tau in Alzheimer’s disease: implications for primary prevention, *Brain communications* 2 (1) (2020) fcaa007.